Acta Crystallographica Section B
Structural Science
ISSN 0108-7681

Mullite-type $Ga_4B_2O_9$: structure and order–disorder phenomenon

Rihong Cong,[a] Tao Yang,[a] Kuo Li,[a] Hongmei Li,[a] Liping You,[b] Fuhui Liao,[a] Yingxia Wang[a]* and Jianhua Lin[a]*

[a]Beijing National Laboratory for Molecular Sciences, State Key Laboratory of Rare Earth Materials Chemistry and Applications, College of Chemistry and Molecular Engineering, Peking University, Beijing 100871, People's Republic of China, and [b]Electron Microscopy Laboratory, School of Physics, Peking University, Beijing 100871, People's Republic of China

Correspondence e-mail: wangyx@pku.edu.cn, jhlin@pku.edu.cn

Received 9 September 2009
Accepted 6 January 2010

$Ga_4B_2O_9$, an aluminium-free mullite-type compound, was prepared by a boric-acid flux method and its structure was determined using powder X-ray diffraction techniques, in combination with transmission electron microscopy, solid-state ^{11}B MAS-NMR and IR spectroscopies. GaO_6 octahedra share edges in a *trans*-manner forming one-dimensional chains along the *b* direction, and the chains are further cross-linked by GaO_5, BO_3 and BO_4 groups into a three-dimensional mullite-type structure. The disorder of the inter-chain groups results in a small unit cell for $Ga_4B_2O_9$ compared with that for $Al_4B_2O_9$, an ordered compound with a superstructure. By deconstructing the structure of $Ga_4B_2O_9$, we were able to identify the fundamental building units and their linking rules which can be used to reconstruct the ordered and disordered structures. For $Ga_4B_2O_9$, we found that the structure is intrinsically disordered within the *ac* plane, but ordered along the *b* axis. The three-dimensional structure can then be constructed by stacking the disordered *ac* sheets along the *b* axis ($\frac{1}{2}b$) with a $\frac{1}{2}a$ shift. The fundamental building units and exclusivity rules identified in this gallium borate mullite may also be useful for understanding other related mullite phases. The structure analysis applying the proposed method is used to recognize the structural features of $Al_4B_2O_9$ and $Al_{18}B_4O_{33}$.

1. Introduction

Mullite is one of the most important phases in ceramics due to its favourable properties, such as low thermal capacity, low thermal expansion, high thermal stability, excellent creep resistance and high corrosion resistance (Burnham, 1964; Angel & Prewitt, 1986; Aksay *et al.*, 1991; Schneider & Komarneni, 2005; Schneider *et al.*, 1994, 2008). Formulated as $Al_{4+2x}Si_{2-2x}O_{10-x}$, with x ranging typically from 0.18 to 0.88 (Fischer *et al.*, 1996), mullite is a coupled substituted product of sillimanite Al_2SiO_5, an end-member where $x = 0$ (Burnham, 1963; Bish & Burnham, 1992). According to the ratio of alumina to silica, there are so-called 3/2-mullite ($3Al_2O_3$–$2SiO_2$) (Saalfeld & Guse, 1981; Balzar & Ledbetter, 1993) and 2/1-mullite ($2Al_2O_3$–SiO_2; Angel *et al.*, 1991; Sadanaga *et al.*, 1962; Delmastro *et al.*, 1992), corresponding to the substitution content $x = 0.25$ and 0.4. Mullites containing boron, the so-called boron mullites (Werding & Schreyer, 1984, 1992, 1996; Griesser *et al.*, 2008; Fischer & Schneider, 2008), include the synthetic compounds $Al_4B_2O_9$ (Scholze, 1956; Mazza *et al.*, 1992; Fischer, Kahlenberg *et al.*, 2008; Wang *et al.*, 2005), $Al_{18}B_4O_{33}$ or Al_5BO_9 (Sokolova *et al.*, 1978; Ihara *et al.*, 1980; Garsche *et al.*, 1991; Wada *et al.*, 1993), as well as the minerals

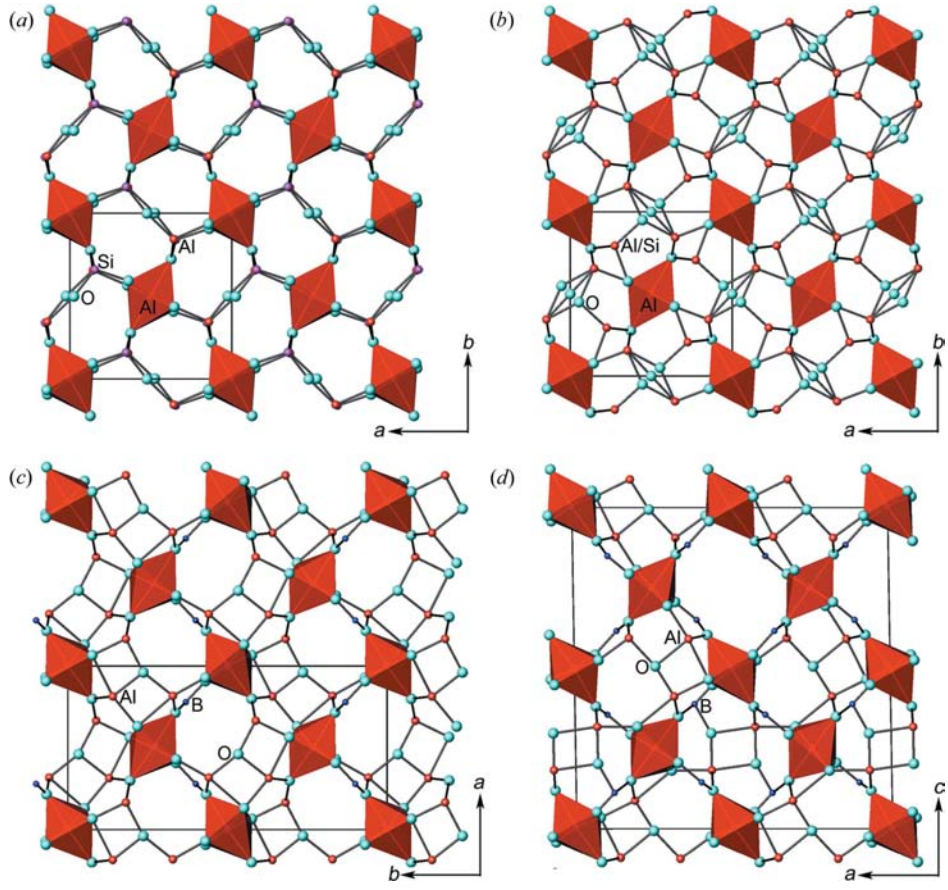

Figure 1
Comparison of structures: (*a*) sillimanite; (*b*) (3/2 or 2/1)-mullite; (*c*) $Al_{18}B_4O_{33}$; (*d*) $Al_4B_2O_9$ (small, medium and large spheres represent B, Al/Si and O atoms, respectively; octahedra are AlO_6).

boralsilite $Al_{16}B_6Si_2O_{37}$ (Grew *et al.*, 1998, 2008; Peacor *et al.*, 1999) and boromullite $Al_9BSi_2O_{19}$ (Buick *et al.*, 2008).

The mullite structures feature linear edge-sharing AlO_6 octahedral chains that are cross-linked by various inter-chain groups as shown in Fig. 1. Sillimanite is a stoichiometric compound in which the AlO_4 and SiO_4 tetrahedra are ordered as inter-chain groups (Fig. 1*a*; Burnham, 1963; Bish & Burnham, 1992). The substitution of Al^{3+} for Si^{4+} introduces oxygen vacancies and as a consequence more extensive linkage of the inter-chain groups. For example, in the (3/2 or 2/1)-mullite, three inter-chain groups are condensed forming T_3O groups (T = randomly distributed Al or Si) or T_2O groups, as shown in Fig. 1(*b*) (Balzar & Ledbetter, 1993; Angel *et al.*, 1991; Voll *et al.*, 2001; Paulmann, 1996; Schmücker *et al.*, 2005). Incorporation of boron into mullites results in more complex structures because of triangular and tetrahedral coordination geometries of boron with O atoms. For example, in $Al_{18}B_4O_{33}$ (Fig. 1*c*) the octahedral chains are linked by triangular BO_3, tetrahedral AlO_4 and bipyramidal AlO_5 groups (Garsche *et al.*, 1991), while in boralsilite $Al_{16}B_6Si_2O_{37}$, they are linked by Si_2O_7, BO_4, BO_3 and AlO_5 groups (Peacor *et al.*, 1999). The structure of $Al_4B_2O_9$ is closely related to $Al_{16}B_6Si_2O_{37}$, and the further replacement of Si by B atoms gives rise to the corresponding cross-linking groups AlO_4, AlO_5, BO_3 and BO_4, as shown in Fig. 1(*d*) (Fischer, Kahlenberg *et al.*, 2008).

Isostructural gallium mullites should exist, because Al^{3+} and Ga^{3+} have comparable ionic radii (Al^{3+}: 0.39, 0.48 and 0.54 Å and Ga^{3+}: 0.47, 0.55 and 0.62 Å for CN = 4, 5 and 6; Shannon, 1976) and similar chemical properties. Gelsdorf *et al.* (1958) reported the synthesis of gallium-bearing mullites $Al_4Ga_2Si_2O_{13}$ and $Ga_6Ge_2O_{13}$, but they were not successful in synthesizing a Ga analogue of silicate mullite. However, few mullite-type compounds reported to date contain gallium, for example $Ga_6Ge_2O_{13}$ (Voll *et al.*, 2001; Schneider & Werner, 1982; Schneider, 1981), $Ga_4Bi_2O_{10}$ (Müller-Buschbaum & de Beaulieu, 1978; Filatov *et al.*, 2006; Beran *et al.*, 2008) and alkaline gallates $Ga_6M_{0.67}O_{9.33}$ (M = K, Na, Rb; Angerer, 2001; Fischer *et al.*, 2001). As for mullite-type gallium borates, no information is available and only the sillimanite-type compound $PbGaBO_4$ has been reported (Park & Barbier, 2001).

The typical synthesis process for mullite-type materials is conventional solid-state reaction at high temperature, generally above 1273 K. The sol–gel process, co-precipitation, spray hydrolysis, hydrothermal processes and even the chemical vapor deposition method have also been employed to promote the formation of mullites and/or to improve their microstructure and properties (Schneider & Komarneni, 2005; Schneider *et al.*, 2008; Griesser *et al.*, 2008). It is well known that boric acid may dehydrate stepwise and polymerizes to metaboric acid and then to boron oxide in an open vessel, while in a closed system it melts at $\sim$ 443 K and can, therefore, serve as a reaction medium at low temperature (Wells, 1975). By using a boric-acid flux method, we were able to obtain a series of new borates, including PKU-n (n = 1–8; here PKU is the abbreviation of Peking University) and rare-earth polyborates (Lu *et al.*, 2001; Ju *et al.*, 2003, 2004; Yang *et al.*, 2007; Gao *et al.*, 2008; Li *et al.*, 2002, 2003). PKU-1 is an interesting aluminoborate $[HAl_3B_6O_{12}(OH)_4]$ with 18-ring tunnels constructed by AlO_6 octahedra (Ju *et al.*, 2003). In the effort to synthesize the gallium analogue (GaPKU-1), $Ga_4B_2O_9$, a new compound with a mullite-type structure appeared. $Ga_4B_2O_9$ is a binary phase in the system of Ga_2O_3–B_2O_3; and from previous studies the only known binary gallium borate is $GaBO_3$ (Rudenko, 1995; Dotsenko *et al.*, 1996; Pelzer & Muller, 2001).

$Ga_4B_2O_9$ consists of *trans* edge-sharing GaO_6 infinite chains that are interconnected by inter-chain units GaO_5, BO_3 and BO_4. As we will show in this paper, the inter-chain groups in $Ga_4B_2O_9$ are heavily disordered. In the structure analysis, we identified several fundamental building units (BUs) in the structure of $Ga_4B_2O_9$ and by using these building units we were able to reconstruct the ordered and disordered structure models of boron mullites, and then to provide a comprehensive understanding for the ordered and disordered boron-mullite structures.

2. Experimental

2.1. Synthesis

The boric-acid flux method and solid-state reaction were used to synthesize $Ga_4B_2O_9$. For the boric-acid flux method, β-Ga_2O_3 was used as the gallium source and pre-treated by the following process to enhance its reactivity: 5 mmol of β-Ga_2O_3 (0.4686 g), 1 ml concentrated HNO_3 and 3 ml of HCl were placed into a 50 cm^3 Teflon® container with a stainless steel shell. The autoclave was put into an oven at 453 K for 12 h. After cooling to room temperature, the autoclave was opened, and 50–300 mmol H_3BO_3 was added to the container. The vessel was sealed again and kept in an oven at 488 K for 8–12 d. The white powder products were obtained and washed thoroughly with hot water (353 K) to remove the residual boric acid. The ratio of Ga/B of the reactants showed no significant influence on the formation of $Ga_4B_2O_9$, but the pre-treatment of Ga_2O_3 by aqua regia was necessary and the addition of a small amount of water (1–5 drops) to the reaction system significantly improved the crystallization of the product. The scanning electron microscopy (SEM) image in Fig. 2 shows that the rod products are well crystallized.

In a solid-state reaction, a mixture of Ga_2O_3 and H_3BO_3 was fully ground and reacted at 873–973 K for $\sim$ 5–10 h, but the expected product was not formed. When $Ga(NO_3)_3{\cdot}xH_2O$ was used as the source of gallium, $Ga_4B_2O_9$ was obtained. The typical process is as follows: a stoichiometric mixture of $Ga(NO_3)_3{\cdot}xH_2O$ and H_3BO_3 (with 1 mol% excess H_3BO_3) was grounded fully and calcined at 923 K for 5 h. The crystallinity of the product was quite poor in comparison with that from the boric-acid method (Fig. S1 of the supplementary material[1]). Longer annealing time (> 10 h at 923 K) or higher reaction temperature (973 K) resulted in a decomposition of $Ga_4B_2O_9$ to $GaBO_3$ and Ga_2O_3 (Fig. S2).

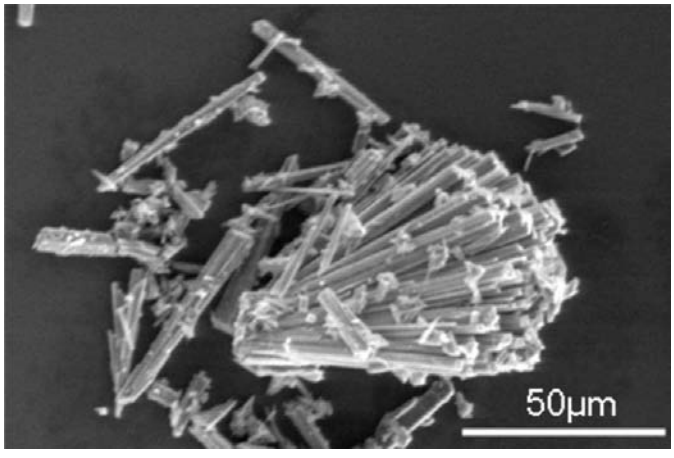

Figure 2
SEM image of $Ga_4B_2O_9$ synthesized by the boric-acid flux method.

2.2. Characterization

The chemical analysis of gallium and boron was conducted by the inductively coupled plasma emission spectroscopy (ICP-ES) method on an ESCALAB2000 analyzer and showed a result of Ga:B = 1.96:1 (molar ratio). The thermal stability of the samples was analyzed with the combined thermogravimetric analysis (TGA) and differential scanning calorimetry (DSC) on a Q600SDT thermogravimetric analyzer, in nitrogen atmosphere with a heating rate of 10 K min^{-1} from 303 to 1273 K. The IR spectrum was measured on a NICOLET iN10 MX instrument. Electron diffraction (ED) studies were performed on a Tecnai F30 transmission electron microscope under 300 kV. SEM micrographs were taken on a *QUANTA* 200FEG. Solid-state ^{11}B magic-angle spinning (MAS) NMR spectra were recorded on a Varian Unity Plus-400 spectrometer under spinning speed 20 kHz using $BF_3{\cdot}OEt_2$ as the standard.

Powder X-ray diffraction data for structure analysis were collected at room temperature on a Bruker D8 Advance diffractometer in Debye–Scherrer geometry, using Ge-monochromized Cu $K\alpha$ radiation (λ = 1.54059 Å), a capillary sample holder and a position-sensitive detector (4° 2θ open angle). The data were recorded from 8 to 120° with step size 0.0144° with 40 s per step under tube conditions 40 kV and 40 mA. The indexing of the powder X-ray diffraction (XRD) data was performed using the program *PowderX* (Dong, 1999). The structure model of $Ga_4B_2O_9$ was established *ab initio* by the simulated annealing method and refined by Rietveld analysis with the program *TOPAS* (Bruker, 2003). Soft restraints were applied to the displacement parameters of the atoms.

Supporting materials include an SEM image of $Ga_4B_2O_9$ synthesized by solid-state reaction, X-ray diffraction patterns of the samples synthesized under different conditions, a Rietveld plot of the powder X-ray diffraction pattern of $Ga_4B_2O_9$ using the ordered model, and the structure analysis for $Al_{16}B_6Si_2O_{37}$.

3. Results and discussion

3.1. Thermal stability of $Ga_4B_2O_9$

The TGA–DSC curves of $Ga_4B_2O_9$ (Fig. 3*a*) show an endothermic effect occurring at $\sim$ 1148 K, but no weight loss up to 1273 K. The endothermic peak can be described as an incongruent melting process resulting in the decomposition of

[1] Supplementary data for this paper are available from the IUCr electronic archives (Reference: KD5038). Services for accessing these data are described at the back of the journal.

$Ga_4B_2O_9$ to solid Ga_2O_3 and liquid B_2O_3. Fig. 3(*b*) shows the X-ray diffraction patterns of the $Ga_4B_2O_9$ samples after calcination at different temperatures in a muffle furnace. $Ga_4B_2O_9$ remains up to 973 K, and decomposes to Ga_2O_3 and non-crystalline B_2O_3 above 1023 K.

3.2. Structure determination

The powder X-ray diffraction pattern of $Ga_4B_2O_9$ can be readily indexed with a monoclinic lattice, a = 15.37, b = 5.72, c = 11.00 Å, β = 135.24° and V = 680.0 Å^3. Considering the similarity of Al^{3+} and Ga^{3+}, the structure of $Al_4B_2O_9$ was initially used as a reference model for $Ga_4B_2O_9$ (Fischer, Kahlenberg *et al.*, 2008). $Al_4B_2O_9$ crystallizes in a monoclinic structure with lattice constants a = 14.8056, b = 5.5413, c = 15.0531 Å, β = 90.913° and V = 1234.8 Å^3 in space group $C2/m$. Comparing the two sets of the lattice constants, we can find the relationship between the two structures: $a_{Ga} = 15.4 \simeq c_{Al}$, $b_{Ga} = 5.54$ Å $\simeq b_{Al}$ and $c_{Ga} = 11.0$ Å $\simeq (a_{Al} + c_{Al})/2$. As the cell volume of $Ga_4B_2O_9$ is roughly half that of $Al_4B_2O_9$, we thought that $Ga_4B_2O_9$ might be an analogue of $Al_4B_2O_9$. However, refinement using the $Al_4B_2O_9$ model led to a rather poor fit, indicating that the structure of $Ga_4B_2O_9$ is not a simple disordered analogue of $Al_4B_2O_9$. The electron diffraction (ED; Fig. 4) definitely shows that there are no superstructure reflections in $Ga_4B_2O_9$. The systematic absences of ED and powder X-ray data reveal the possible space groups $C2$, Cm and $C2/m$. The structure model of $Ga_4B_2O_9$ was then established in the space group $C2/m$ using the simulated annealing method with *TOPAS*.

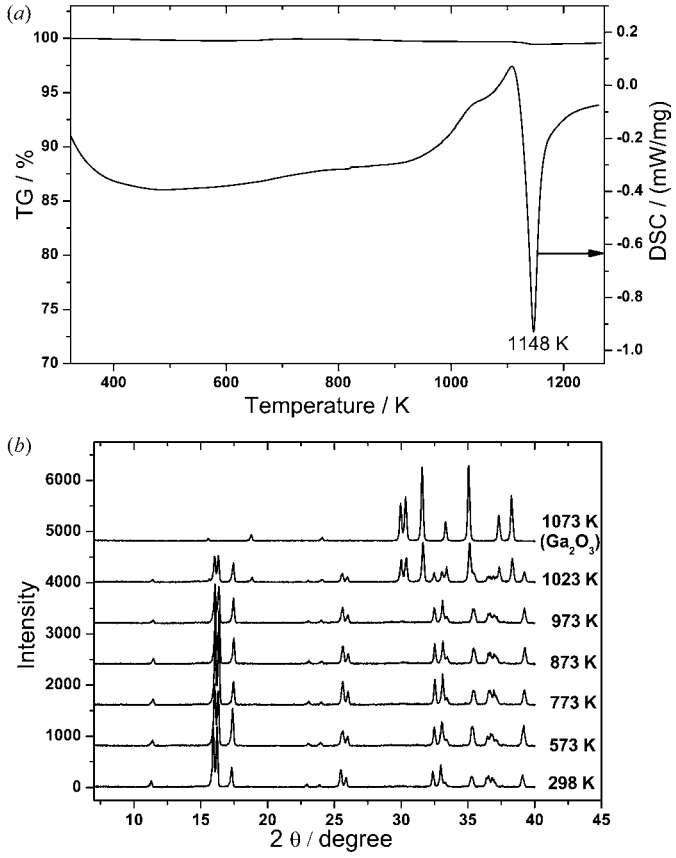

Figure 3
(*a*) TGA–DSC curves for $Ga_4B_2O_9$; (*b*) X-ray diffraction patterns of the sample as synthesized at 298 K and its calcined products at different temperatures.

There are 16 unique sites identified from structure analysis (Ga1–Ga5, O1–O8, B1, B21 and B22); six of them, Ga4, Ga5, B21, B22, O7 and O8, are partially occupied. The unrealistically short distances, for example B21—B22 (0.40 Å), Ga4—Ga5 (1.63 Å) and O7—O7 (0.97 Å), indicate the strong correlation between these positions, thus constrained occupancies, for example $Occ_{B21} + Occ_{B22} = 1$ and $Occ_{Ga4} + Occ_{Ga5} = 1$, were employed in the initial stage of the refinement. The occupancies of the partially occupied atoms (Ga4, Ga5, B21, B22, O7 and O8) were all close to 0.5 during the refinement, so they were fixed to $\frac{1}{2}$ in the final refinement. Another feature of the structure is the coordination variation of B atoms. The IR and ^{11}B MAS-NMR spectra indicate the presence of triangular and tetrahedral coordination of B atoms in the structure (Fig. 5). In ^{11}B MAS-NMR, the broad-band peaking at 2.3 and 12.3 p.p.m. is typical for BO_3 and the sharp peak at *ca* −0.1 p.p.m. originates from the BO_4 group (Fischer, Kahlenberg *et al.*, 2008; Li *et al.*, 1995; Epping *et al.*, 2005; Chan *et al.*, 1998, 1999). During the structure refinement it became clear that B1 is well defined in triangular coordination. B21 and B22, on the other hand, are coordinated in triangular and tetrahedral geometries. Therefore, B21 and B22 were refined using rigid bodies at the initial stage, and then using soft constraints in the final refinement, which led to R_p = 0.063 and R_{wp} = 0.082. Fig. 6 shows the Rietveld refinement plot of the diffraction pattern. The X-ray data collection conditions, crystallographic data and results of Rietveld analysis are summarized in Table 1. Selected bond distances, bond angles and bond-valence sums (BVSs) are listed in Table 2.

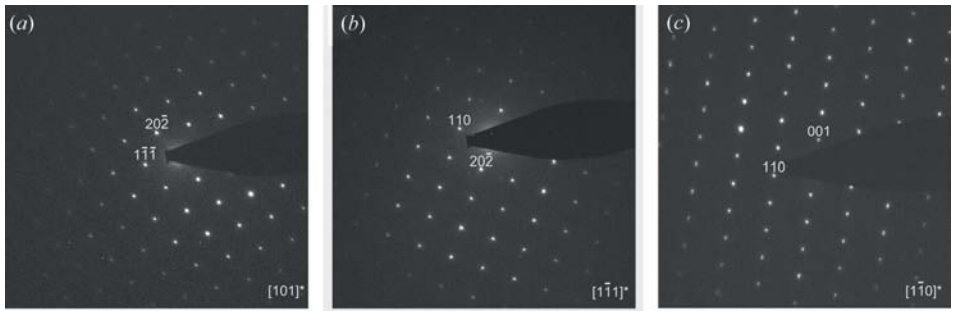

Figure 4
Electron-diffraction patterns of $Ga_4B_2O_9$ along the zones: (*a*) [101], (*b*) [1$\bar{1}$1] and (*c*) [1$\bar{1}$0].

3.3. Structure description and disorder of inter-groups

$Ga_4B_2O_9$ takes a disordered mullite-type structure and can be

Table 1
X-ray data collection conditions, crystallographic data and results of Rietveld analysis for $Ga_4B_2O_9$.

Crystal data	
Chemical formula	$Ga_4B_2O_9$
M_r (g mol^{-1})	444.50
Crystal system, space group	Monoclinic, *C*2/*m*
Temperature (K)	293
a, *b*, *c* (Å)	15.3582 (3), 5.7190 (1), 10.9933 (2)
β (°)	135.2358 (6)
V (Å^3)	679.96 (2)
Z	4
D_x (Mg m^{-3})	4.342
Radiation type	Cu $K\alpha_1$, λ = 1.540596 Å
μ (mm^{-1})	18.56
Specimen shape, size (µm)	Rod, ~ 50 × 1
Data collection	
Diffractometer	Bruker D8 Advance
Specimen mounting	Capillary (0.3 mm)
Data collection mode	Transmission
Scan method	Step
2θ values (°)	$2\theta_{min}$ = 8, $2\theta_{max}$ = 119.9876, $2\theta_{step}$ = 0.0144
Refinement	
R factors and goodness of fit	R_p = 0.063, R_{wp} = 0.082, R_{exp} = 0.040, χ^2 = 4.23
Excluded regions (°)	29.3551–29.8310
Number of data points	7779
Number of parameters	70
Number of restraints	11

Computer programs used: *TOPAS*2.1 (Bruker, 2003).

Table 2
Selected bond distances (Å), and angles (°), and BVS values for $Ga_4B_2O_9$.

GaO_6 octahedra			
Ga1—O2	1.88 (1) ×2	Ga2—O1	1.84 (1) ×2
Ga1—O5	1.99 (1) ×2	Ga2—O3	1.968 (7) ×2
Ga1—O4	2.001 (5) ×2	Ga2—O6	2.073 (9) ×2
BVS	3.29	BVS	3.33
GaO_5 bi-pyramids			
Ga3—O5	1.904 (6) ×2	Ga4—O2	1.79 (2)
Ga3—O7	1.78 (4) or 1.91 (3)	Ga4—O7	1.81 (2)
Ga3—O1	1.93 (1)	Ga4—O6	1.958 (7) ×2
Ga3—O2	2.31 (1)	Ga4—O1	2.14 (2)
BVS	2.92 or 2.66	BVS	3.07
Ga5—O8	1.82 (2)		
Ga5—O8	1.97 (4)		
Ga5—O6	2.012 (7) ×2		
Ga5—O2	2.04 (2)		
BVS	2.67		
BO_3 triangles			
B1—O4	1.31 (2)	O4—B1—O6	125.5 (4) ×2
B1—O6	1.44 (2) ×2	O6—B1—O6	108.6 (25)
BVS	2.84		
B21—O3	1.30 (1)	O3—B21—O5	124.4 (2) ×2
B21—O5	1.420 (6) ×2	O5—B21—O5	111.2 (4)
BVS	2.96		
BO_4 tetrahedra			
B22—O3	1.412 (8)	O3—B22—O8	107.2 (7)
B22—O8	1.48 (4)	O8—B22—O5	105.2 (3) ×2
B22—O5	1.446 (7) ×2	O5—B22—O5	108.3 (6)
BVS	3.27	O5—B22—O3	115.0 (4) ×2

described as chains of edge-sharing GaO_6 octahedra parallel to the *b* axis that are cross-linked by three different inter-chain groups, *i.e.* GaO_5, BO_3 and BO_4. In Fig. 7(*a*) we show a projection of $Ga_4B_2O_9$ along the *b* axis. In the structure, the octahedral chains are well defined and all the atoms within the chains are fully occupied (Ga1 and Ga2). On the other hand, the inter-chain groups except B1 are highly disordered, much more than in other mullite-type compounds (Fig. 1), in which disorder of the inter-chain groups is a common phenomenon.

Ga1 and Ga2 are octahedrally coordinated in the structure of $Ga_4B_2O_9$ with the Ga—O bond distances ranging from 1.84 to 2.07 Å (Table 2). The Ga octahedra (either Ga1 or Ga2) share opposite edges in a *trans*-manner forming the infinite octahedral chains, as shown in Fig. 7(*b*). The octahedral chains are parallel to the *b* axis, with the orientation similar to that in rutile-type structure, but they are independent and interconnected by inter-chain groups in $Ga_4B_2O_9$ (Fig. 7*a*), leading to the formation of the quasi-tetragonal channels along the *b* axis. This quasi-tetragonal channel framework is a fundamental characteristic of mullite-type structures. The inter-chain groups in $Ga_4B_2O_9$ can be divided into two categories: borate groups (BO_3 and BO_4) and GaO_5 groups. The borate groups are regular and the refined B—O bond distances are all in a reasonable range as shown in Table 2, while the gallium atoms (Ga3, Ga4 and Ga5) are all coordinated in trigonal

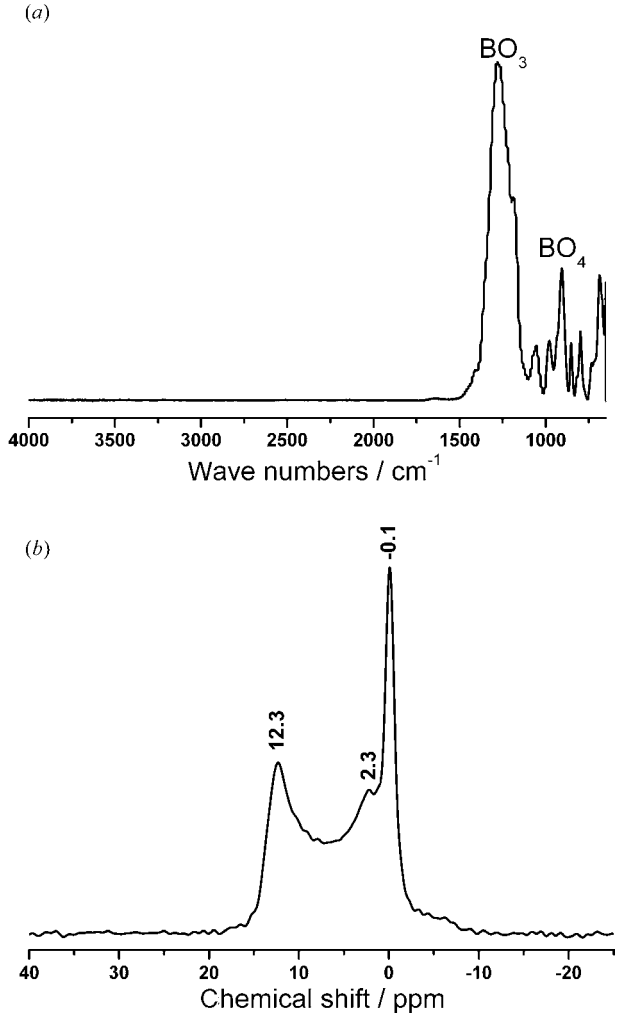

Figure 5
(*a*) IR spectrum and (*b*) ^{11}B MAS-NMR spectrum for $Ga_4B_2O_9$.

pyramidal geometry with Ga—O distances ranging from 1.78 to 2.31 Å. To understand the structure, one can deconstruct the disordered structure into chemically meaningful building units and then address the origin of the disorder phenomenon.

Here, the distinctive building units (BUs) are defined by structure deconstruction analysis. First, we focus on a single sheet perpendicular to the *b* direction as shown Fig. 8(*a*). Four different building units (designated as *A*, *B*, *C* and *D*′) can be readily identified (Fig. 8*b*). Each unit consists of eight octahedra and the inter-chain groups that link the octahedral chains together. It should be noted that they may not be the true fundamental building units in the structure because the disordered inter-chain groups have not yet been considered. *A* is a true fundamental building unit in which the octahedral chains are linked by both triangular borate groups (B1) and GaO_5 (Ga3). The triangularly coordinated boron atom (B1) is fully occupied and shares three O atoms with two neighbouring octahedral chains. Since the O7 atom, which is linked to Ga3 to complete the penta-coordination of Ga with other four O atoms, is located in the neighbouring units of *A* and does not belong to the unit *A*, it is not shown in the figure expression of BU-*A* (Fig. 8*a*). On the other hand, *B*, *C* and *D*′ are all quasi-building units, and here they are designated as qBU-*B*, qBU-*C* and qBU-*D*′. qBU-*B* contains B1 triangular borate groups and disordered borate groups (B21 and B22). The B21 triangular and B22 tetrahedral groups share three common O atoms from the adjacent octahedral chains, and meanwhile B22 bonds to an additional half-occupied O8 in the channel to complete the tetrahedral coordination. Obviously, B21 and B22 in qBU-*B* cannot appear simultaneously, thus, microscopically, four different fundamental building units, *i.e.* BU-B_1, BU-B_2, BU-B_3 and BU-B_4, can be derived from qBU-*B*. As shown in Fig. 9, the inter-chain groups are two triangular (B1) and two tetrahedral (B22) borate groups in BU-B_1, and are all triangular borates in BU-B_4; BU-B_2 and BU-B_3 both consist of three BO_3 and one BO_4, but the orientations of BO_4 are different.

qBU-*C* contains two different gallium trigonal bipyramids (Ga3 and Ga4), as shown in Fig. 8(*b*). Ga3 is fully occupied and shares four O atoms with two neighbouring octahedral chains. The fifth Ga3—O bond is the connection of the Ga3 atom with O7. There are two O7 atoms near the Ga3 atom with distances of 1.78 and 1.91 Å. However, the O7 positions are only half-occupied and then we only need to take one of the connections into account. Ga4, on the other hand, is also a half-occupied position surrounded by four O atoms from the octahedral chains and one additional O7 atom in the channel. Regarding the short O7—O7 distance (0.97 Å), Ga4 atoms cannot appear as a pair in the tetragonal channel; thus qBU-*C* may also be deconstructed into

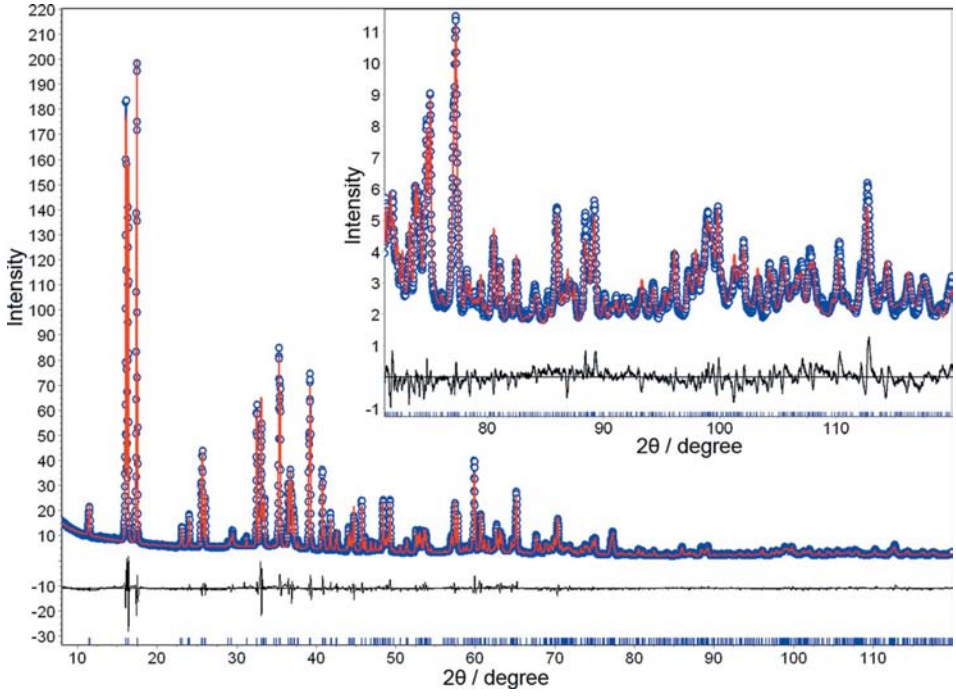

Figure 6
Rietveld plot of the powder X-ray diffraction profile of $Ga_4B_2O_9$; the enlarged insert shows the good fit of the high-angle section. The circle symbol (○) represents the observed data and the solid line is the calculated pattern; the difference curve is shown below the diffraction profile and the short vertical bars are the reflection positions.

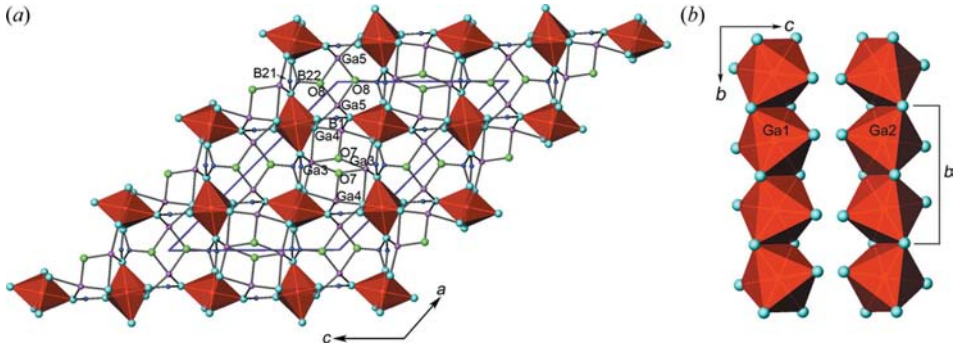

Figure 7
(*a*) Projection of the structure of $Ga_4B_2O_9$ along the *b* direction; (*b*) octahedral chains along the *b* axis.

two building units, *i.e.* BU-T_1 and BU-T_2 (T denotes the Ga_3O_{11} trimer formed in the units). As shown in Fig. 9, in each unit three GaO_5 trigonal bipyramids (two from Ga3 and one from Ga4) form a Ga_3O_{11} trimer *via* the common O7 atom.

qBU-D' contains both borate groups (B21 or B22) and gallium (Ga5) trigonal bipyramid groups (Fig. 8*b*). Two Ga5 trigonal bipyramids in the channel share a common edge (O8—O8) forming a Ga_2O_8 dimer. Although the O8—O8 distance is relatively short (2.26 Å), it is not unreasonable and, in fact, there are a number of examples, such as andalusite (Burnham & Buerger, 1961) and boralsilite (Peacor *et al.*, 1999), which do contain such short O—O contacts (2.23 and 2.26 Å) in edge-sharing trigonal bi-pyramids. We already knew that B21 and B22 cannot appear simultaneously and O8 is essential for the formation of tetrahedral borate (B22). Therefore, qBU-D' can be sorted into two building units: one contains tetragonal B22 and Ga5 dimer (BU-D), and the other contains only triangularly coordinated B21, while leaving the Ga5 and O8 positions empty (BU-E), as shown in Fig. 9.

We have already identified all possible fundamental building units in $Ga_4B_2O_9$. To construct the structure, one could re-combine these building units in appropriate ways. It should be noted that the connection of the building units is not arbitrary, but there are a number of rules that exclude certain types of connections. Looking at the *ac* sheet shown in Fig. 8(*a*) and focusing on the [101] direction, one could see that T_1, T_2, D and E, as well as A and B_n (n = 1–4), are connected, respectively, forming two independent chains. A and B_n (n = 1–4) all contain BO_3 (B1) as the inter-chain groups in the [101] direction, so there is no exclusivity rule. The chains containing T_1, T_2, D and E should obey the following rules:

(i) Ga4 and Ga5 should not appear simultaneously as neighbours.

A consequence of the first exclusivity rule is that T_1 and T_2 can only link to E and D on one side, which leads to an unique sequence, $T_1DT_2ET_1$, along the [101] direction. In the *c* direction, we could also see two independent chains; one consists of A, T_1 and T_2 and the other consists of D, E and B_n (n = 1–4). The connection of A to T_1 and T_2 is arbitrary without restriction. The chains consisting of D, E and B_n (n = 1–4), on the

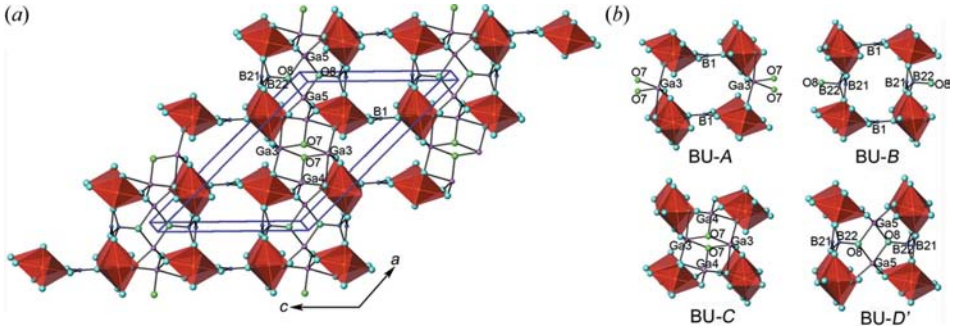

Figure 8
(*a*) A single sheet perpendicular to the *b* direction isolated from the structure of $Ga_4B_2O_9$; (*b*) building unit and quasi-building units of $Ga_4B_2O_9$.

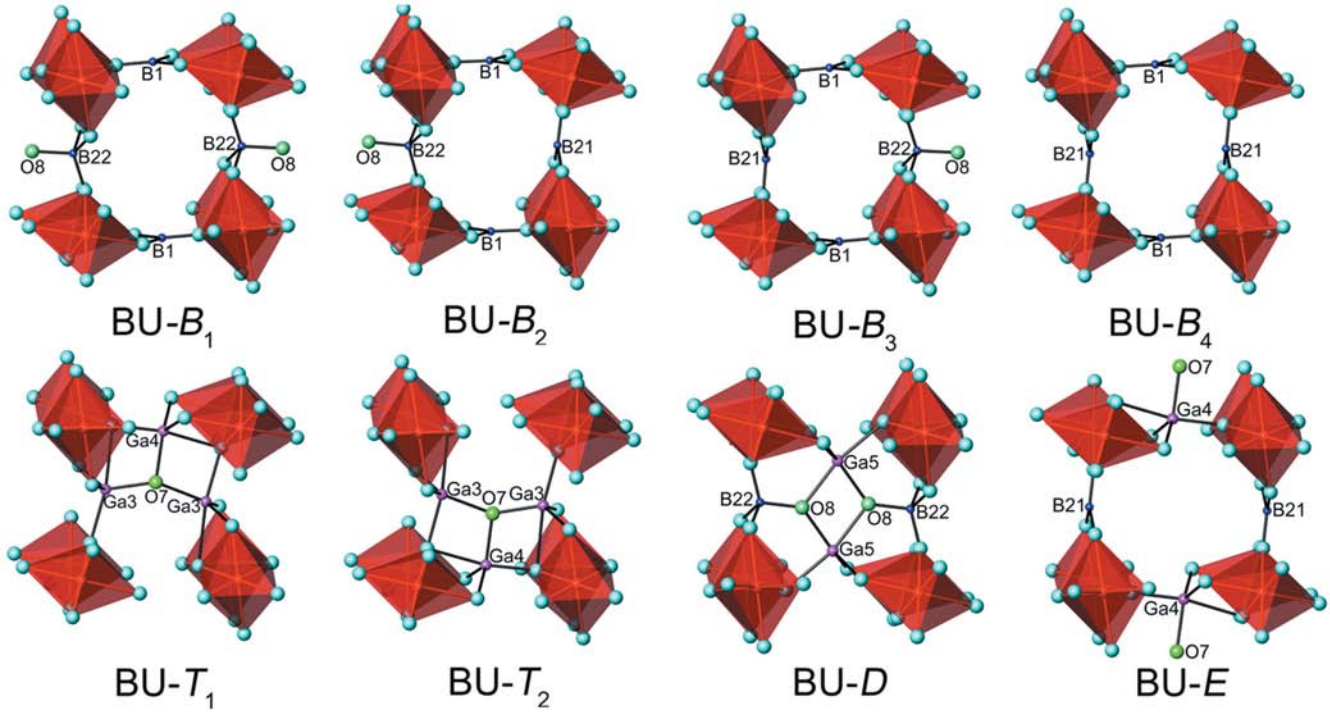

Figure 9
Fundamental building units in the structure of $Ga_4B_2O_9$.

other hand, should obey the second rule.

(ii) B21 and B22 should not appear simultaneously as neighbours.

Consequently, the connections of D and E to B_n (n = 1–4) are unidirectional, because D can only be connected to B_1, B_2 and B_3 through BO_4, and E can only link to B_2, B_3 or B_4 *via* BO_3. For example, DB_2 is valid, but the reverse connection B_2D is prohibited. These exclusivity rules significantly reduce the possible linkages between the fundamental building units.

To build up the structure of $Ga_4B_2O_9$, we start from the chain T_1DT_2E along the [101] direction (Fig. 10*a*), since it is uniquely defined by the first exclusivity rule. To expand the sheet along the c direction, one should consider two independent linkages, *i.e.* one consists of A, T_1 and T_2 and the other consists of D, E and B_n (n = 1–4). We knew that the connection of T_m (m = 1, 2) and D is exchangeable, thus both T_1 and T_2 can be connected to A as shown in Figs. 10(*b*) and (*c*). However, further expanding will have multiple choices: A may connect either T_1 or T_2, which leads to four possible linkages, T_1AT_1, T_2AT_2 or T_1AT_2, T_2AT_1. For the chain consisting of D, E and B_n (n = 1–4), the linkages follow the second exclusivity rule, thus D can be connected to either B_1 or B_2, while E can be connected to either B_3 or B_4. Further connections are uniquely defined, *i.e.* DB_1D, DB_2E, EB_3D and EB_4E, according to the second exclusivity rule. One could imagine that the further extension along the c axis will create more possible different linkages. For example, DB_1D and EB_3D may connect to either B_1 or B_2, and DB_2E and EB_4E may connect to either B_3 or B_4. Although the first and second exclusivity rules can significantly reduce the rational linkages, the probability of the linkages increases enormously as the *ac* sheet expands along the c axis, which leads to a highly disordered *ac* sheet in the structure. Fig. 11 shows, in a concise expression, the possible ways that the *ac* sheet can be expanded along the c axis.

We have reproduced the *ac* sheet in the structure of $Ga_4B_2O_9$ using the fundamental building units and demonstrated that it is intrinsically disordered owing to the numerous possible linkages of the fundamental building units. The three-dimensional structure of $Ga_4B_2O_9$ can be obtained by stacking the *ac* sheets along the b axis in a step of $\frac{1}{2}b$ and then shifting along the a axis in $\frac{1}{2}a$. Therefore, $Ga_4B_2O_9$ could be regarded as a two-dimensional intrinsic disordered structure, *i.e.* it is disordered within the *ac* plane and ordered along the b axis.

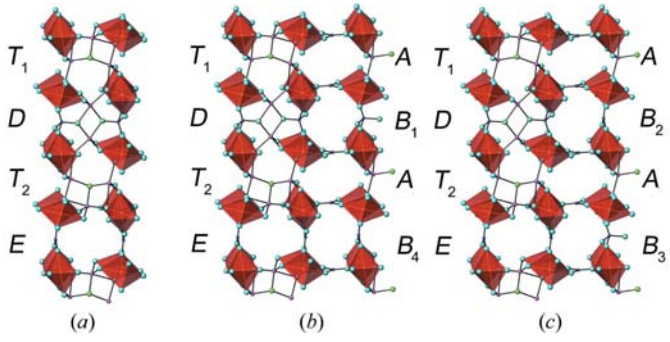

Figure 10
(*a*) The uniquely defined chain of T_1DT_2E along the [101] direction; (*b*) and (*c*) two examples of the possible extension modes along the c direction.

3.4. Further review on the structures of $Al_4B_2O_9$ and $Ga_4B_2O_9$

The structure analysis by the deconstruction and the recombination of building units enables us to have a comprehensive understanding of the order–disorder phenomenon in $Ga_4B_2O_9$. Although the direct use of the structure model of $Al_4B_2O_9$ in the structure refinement of $Ga_4B_2O_9$ did not work well, the two structures have much in common. In order to learn the relation between these two structures, we re-study the structure of $Al_4B_2O_9$ applying the fundamental building units. The structure of $Al_4B_2O_9$ was first reported in the orthorhombic space group *Pbam* (Mazza *et al.*, 1992), but a recent study suggested a monoclinic structure with lattice constants a = 14.8056 (7), b = 5.5413 (6), c = 15.0531 (6) Å, β = 90.913 (2)° and V = 1234.8 (3) Å^3, in the space group of *C*2/*m* (Fischer, Kahlenberg *et al.*, 2008). Fischer *et al.* proposed two models for $Al_4B_2O_9$, and the main difference between these two models is the treatments of two O atoms: O5′ and O10. One model has both atoms in half occupancies (Fig. 1*d*), and the other contains fully occupied O10, but without the O5′ atom (Fischer, Kahlenberg *et al.*, 2008). The addition of the O5′ atom to the structure during the refinement was useful in compensating the electron density in the corresponding positions in the channel (Fig. 1*d*). However, as a terminal atom, the O5′ atom only weakly connects to a B atom with a distance of 1.87 Å, which somehow looks strange. The authors pointed out that the details of the structure might be too complex to be solved by Rietveld analysis. In order to highlight the structure feature and to simplify the structure description, we take the ordered model for the structure analysis.

In the structure of $Al_4B_2O_9$, AlO_6 octahedral chains (Al5, Al6, Al7) are cross-linked by inter-chain groups, AlO_4 (Al2 and Al4), AlO_5 (Al1 and Al3), BO_3 (B1, B3, B4) and BO_4 (B2). The comparable b parameters reflect the similar extension of the characteristic octahedral chains, while the order–disorder arrangement of the inter-groups causes the difference of these two structures. In the structure of $Al_4B_2O_9$, the distribution of the inter-groups is more ordered. The inter-chain units in $Al_4B_2O_9$ are AlO_4, AlO_5, BO_3 and BO_4, but only

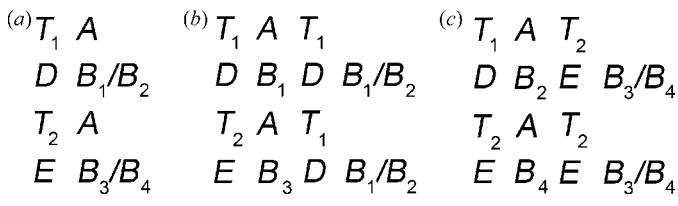

Figure 11
Extension of the *ac* sheet along the c direction starting from the T_1DT_2E chain.

GaO_5, BO_3 and BO_4 in $Ga_4B_2O_9$. Al1 and Al3 are five-coordinated, having similar local environments to those of Ga_4O_5 and Ga_5O_5 in $Ga_4B_2O_9$, but without disordered distribution. Al2 and Al4 in $Al_4B_2O_9$ correspond to Ga3 in $Ga_4B_2O_9$. Ga_3O_5 is a highly distorted bi-pyramid with four short and one long Ga—O bond. Al2 and Al4 are basically four-coordinated, but with an additional longer bond to O8 (2.23 Å) and O2 (2.36 Å), respectively (Fischer, Kahlenberg *et al.*, 2008). In order to elucidate the relationship between the structures of $Al_4B_2O_9$ and $Ga_4B_2O_9$, the long bonds of Al2—O8 and Al4—O2 are taken into consideration, which means that these two atoms are also five-coordinated. Concerning the inter-groups BO_3 (B1, B3, B4) and BO_4 (B2), all are in a regular connection. Accordingly, we can use the fundamental building units identified in $Ga_4B_2O_9$ to build the structure of $Al_4B_2O_9$. Since the distribution of borate groups is ordered, there are no B_1 and B_4 units in $Al_4B_2O_9$. In fact, it is the absence of B_1 and B_4 building units that leads to the ordered connectivity of the

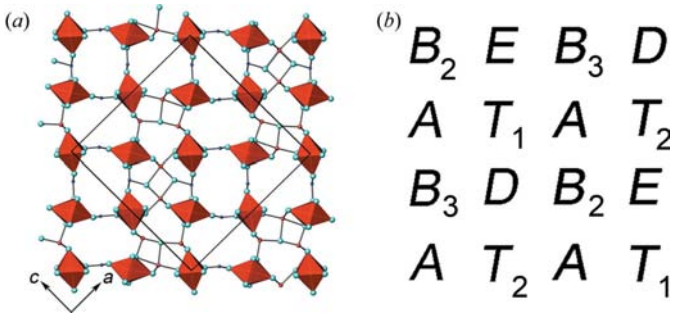

Figure 12
(*a*) The *ac* sheet in the structure of $Al_4B_2O_9$; (*b*) the ordered sheet in $Al_4B_2O_9$ constructed by fundamental building units.

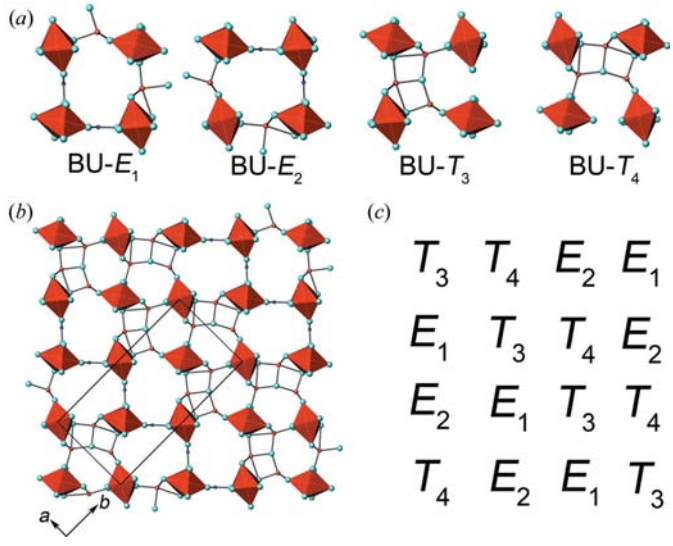

Figure 13
(*a*) Fundamental building units in the structure of $Al_{18}B_4O_{33}$; (*b*) the mono-*ac* sheet isolated from the structure of $Al_{18}B_4O_{33}$; (*c*) reconstruction of the *ab* sheet in $Al_{18}B_4O_{33}$ by the fundamental building units.

building units in the structure of $Al_4B_2O_9$. Fig. 12(*a*) shows an *ac* sheet isolated from the structure of $Al_4B_2O_9$. Starting from the uniquely defined T_1DT_2E chain along the [101] direction and considering the second exclusivity rule, we know that *D* can only link to B_2 and then to *E*, which leads to a uniquely defined chain, DB_2EB_3D, along the $[10\bar{1}]$ direction. Similarly, the chain starting from *E* should be EB_3DB_2E as shown in Fig. 12(*b*). Applying the first exclusivity rule, the other $[10\bar{1}]$ chains consisting of *A*, T_1 and T_2 are all uniquely defined, since the connections of *D* and *E* to T_1 and T_2 are all unidirectional. Therefore, the *ac* sheet in the structure of $Al_4B_2O_9$ is well defined as an ordered plane. The two-dimensional unit cell shown in Fig. 12(*b*) reproduces the real cell of $Al_4B_2O_9$ nicely. The three-dimensional structure can then be formed by stacking the *ac* sheet along the *b* axis ($\frac{1}{2}b$) by a shift of $\frac{1}{2}a$ between neighbouring sheets.

The structure of $Al_{18}B_4O_{33}$ contains different building units. The structure of $Al_{18}B_4O_{33}$ is ordered, and the octahedral chains are cross-linked by inter-chain groups BO_3, AlO_4 and AlO_5, as shown in Fig. 1(*c*) (Garsche *et al.*, 1991). A single sheet perpendicular to the *b* direction can be extracted, as shown in Fig. 13(*a*). Four kinds of fundamental building units: BU-E_1, E_2, T_3 and T_4 can be identified, as shown in Fig. 13(*b*). In this structure, E_1 and E_2, T_3 and T_4 can connect to each other respectively, while T_3 only links to E_1 and T_4, and T_4 to E_2 and T_3. The combination of these building units gives a unique $T_3E_1E_2T_4$ chain along the [110] direction. The extension of the chain along the $[\bar{1}10]$ direction following the connection rules gives rise to the *ab* sheet, as shown in Fig. 13(*c*). The neighbouring *ab* sheets along the *c* axis are related by a $\frac{1}{2}a$ shift. Another example, $Al_{16}B_6Si_2O_{37}$, which is more complex, is presented in the supporting information.

4. Conclusions

$Ga_4B_2O_9$ is a new anhydrous gallium borate crystallizing in a mullite-type structure, where edge-sharing GaO_6 chains along the *b* axis are cross-linked by GaO_5, BO_3 and BO_4 units into three-dimensional structure. The octahedral chains in the structure are ordered and the inter-chain groups are disordered. By deconstructing the disordered structure of $Ga_4B_2O_9$, we were able to identify the fundamental building units and two exclusivity rules that govern the possible connections of the building units, which can be used to interpret the ordered and disordered phenomenon in the structure. The disorder of $Ga_4B_2O_9$ within the *ac* plane is intrinsic, due to the many possible linkages of the fundamental building units. On the other hand, $Al_4B_2O_9$, which also crystallizes in a similar mullite structure, represents another case that is ordered. Comparing these two structures, the only difference is the absence of the building units B_1 and B_4 in $Al_4B_2O_9$, which significantly reduces the variety of the possible linkages between the building units and leads to an intrinsically ordered structure. Order and disorder phenomenon are common in mullites, which often makes these structures difficult to understand. The fundamental building units and exclusivity rules identified in this study may provide a useful

tool to understand the structures of other mullite type compounds, although the building units and exclusivity rules may be different.

This work was supported by the National Natural Science Foundation of China.

References

Aksay, I. A., Dabbs, D. M. & Sarikaya, M. (1991). *J. Am. Ceram. Soc.* **74**, 2343–2358.

Angel, R. J., McMullan, R. K. & Prewitt, C. T. (1991). *Am. Mineral.* **76**, 332–342.

Angel, R. J. & Prewitt, C. T. (1986). *Am. Mineral.* **71**, 1476–1482.

Angerer, P. (2001). PhD Thesis. University of Hannover, Germany.

Balzar, D. & Ledbetter, H. (1993). *Am. Mineral.* **78**, 1192–1196.

Beran, A., Libowitzky, E., Burianek, M., Muhlberg, M., Pecharroman, C. & Schneider, H. (2008). *Cryst. Res. Technol.* **43**, 1230–1239.

Bish, D. L. & Burnham, C. W. (1992). *Am. Mineral.* **77**, 374–379.

Bruker AXS (2003). *TOPAS*, Version 2.1. Bruker AXS, Karlsruhe, Germany.

Buick, I., Grew, E. S., Armbruster, T., Medenbach, O., Yates, M. G., Bebout, G. E. & Clarke, G. L. (2008). *Eur. J. Mineral.* **20**, 935–950.

Burnham, C. W. (1964). *Carnegie Institute of Washington Yearbook*, **63**, 223–227.

Burnham, C. W. (1963). *Z. Kristallogr.* **118**, 127–148.

Burnham, C. W. & Buerger, M. J. (1961). *Z. Kristallogr.* **115**, 269–290.

Chan, J. C. C., Bertmer, M. & Eckert, H. (1998). *Chem. Phys. Lett.* **292**, 154–160.

Chan, J. C. C., Bertmer, M. & Eckert, H. (1999). *J. Am. Chem. Soc.* **121**, 5238–5248.

Delmastro, A., Gozzelino, G., Mazza, D., Vallino, M., Busca, G. & Lorenzelli, V. (1992). *J. Chem. Soc. Faraday Trans.* **88**, 2065–2070.

Dong, C. (1999). *J. Appl. Cryst.* **32**, 838.

Dotsenko, V. P., Efryushina, N. P. & Berezovskaya, I. V. (1996). *Mater. Lett.* **28**, 517–520.

Epping, J. D., Strojek, W. & Eckert, H. (2005). *Phys. Chem. Chem. Phys.* **7**, 2384–2389.

Filatov, S. K., Krivovichev, S. V., Aleksandrova, Y. V., Bubnova, R. S., Egorysheva, A. V., Burns, P., Kargin, Yu. F. & Volkov, V. V. (2006). *Russ. J. Inorg. Chem.* **51**, 878–883.

Fischer, R. X., Kahlenberg, V., Voll, D., MacKenzie, K. J. D., Smith, M. E., Schnetger, B., Brumsack, H. J. & Schneider, H. (2008). *Am. Mineral.* **93**, 918–927.

Fischer, R. X., Schmücker, M., Angerer, P. & Schneider, H. (2001). *Am. Mineral.* **86**, 1513–1518.

Fischer, R. X. & Schneider, H. (2008). *Eur. J. Mineral.* **20**, 917–933.

Fischer, R. X., Schneider, H. & Voll, D. (1996). *J. Eur. Ceram. Soc.* **16**, 109–113.

Gao, W. L., Wang, Y. X., Li, G. B., Liao, F. H., You, L. P. & Lin, J. H. (2008). *Inorg. Chem.* **47**, 7080–7082.

Garsche, M., Tillmanns, E., Almen, H., Schneider, H. & Kupcik, V. (1991). *Eur. J. Mineral.* **3**, 793–808.

Gelsdorf, G., Müller-Hesse, H. & Schwiete, H.-E. (1958). *Arch. Eisenhüttenw.* **29**, 513–519.

Grew, E. S., Graetsch, H. A., Pöter, B., Yates, M. G., Buick, I., Bernhardt, H. J., Schreyer, W., Werding, G., Carson, C. J. & Clarke, G. L. (2008). *Am. Mineral.* **93**, 283–299.

Grew, E. S., McGee, J. J., Yates, M. G., Peacor, D. R., Rouse, R. C., Huijsmans, J. P. P., Shearer, C. K., Wiedenbeck, M., Thost, D. E. & Su, S.-C. (1998). *Am. Mineral.* **83**, 638–651.

Griesser, K. J., Beran, A., Voll, D. & Schneider, H. (2008). *Mineral. Petrol.* **92**, 309–320.

Ihara, M., Imai, K., Fukunaga, J. & Yoshida, N. (1980). *Yogyo-Kyokai-Shi*, **88**, 77–84.

Ju, J., Lin, J. H., Li, G. B., Yang, T., Li, H. M., Liao, F. H., Loong, C.-K. & You, L. P. (2003). *Angew. Chem. Int. Ed.* **42**, 5607–5610.

Ju, J., Yang, T., Li, G. B., Liao, F. H., Wang, Y. X., You, L. P. & Lin, J. H. (2004). *Chem. Eur. J.* **10**, 3901–3906.

Li, J., Xia, Sh. P. & Gao, Sh. Y. (1995). *Spectrochim. Acta A*, **51**, 519–532.

Li, L. Y., Jin, X. L., Li, G. B., Wang, Y. X., Liao, F. H., Yao, G. Q. & Lin, J. H. (2003). *Chem. Mater.* **15**, 2253–2260.

Li, L. Y., Lu, P. C., Wang, Y. Y., Jin, X. L., Li, G. B., Wang, Y. X., You, L. P. & Lin, J. H. (2002). *Chem. Mater.* **14**, 4963–4968.

Lu, P. C., Wang, Y. X., Lin, J. H. & You, L. P. (2001). *Chem. Commun.* **13**, 1178–1179.

Mazza, D., Vallinok, M. & Busca, G. (1992). *J. Am. Ceram. Soc.* **75**, 1929–1934.

Müller-Buschbaum, H. & de Beaulieu, D. Ch. (1978). *Z. Naturforsch. B*, **33**, 669–670.

Park, H. & Barbier, J. (2001). *Acta Cryst.* E**57**, i82–i84.

Paulmann, C. (1996). *Phase Transitions*, **59**, 77–90.

Peacor, D. R., Rouse, R. C. & Grew, E. S. (1999). *Am. Mineral.* **84**, 1152–1161.

Pelzer, H. & Muller, F. (2001). *J. Alloys Comp.* **320**, 262–266.

Rudenko, W. (1995). *Kristallografiya*, **40**, 382–384.

Saalfeld, H. & Guse, W. (1981). *Neues Jahrb. Miner. Monatsh.* pp. 145–150.

Sadanaga, R., Tokonami, M. & Takéuchi, Y. (1962). *Acta Cryst.* **15**, 65–68.

Schmücker, M., Schneider, H., MacKenzie, K. J. D., Smith, M. E. & Carroll, D. E. (2005). *J. Am. Ceram. Soc.* **88**, 2935–2937.

Schneider, H. (1981). *Neues Jahrb. Miner. Abh.* **142**, 111–123.

Schneider, H. & Komarneni, S. (2005). *Mullite*. Weinheim: Wiley-VCH.

Schneider, H., Okada, K. & Pask, J. A. (1994). *Mullite and Mullite Ceramics*. Chichester: Wiley.

Schneider, H., Schreuer, J. & Hildmann, B. (2008). *J. Eur. Ceram. Soc.* **28**, 329–344.

Schneider, H. & Werner, H. D. (1982). *Neues Jahrb. Miner. Abh.* **143**, 223–230.

Scholze, H. (1956). *Z. Anorg. Allg. Chem.* **284**, 272–277.

Shannon, R. D. (1976). *Acta Cryst.* A**32**, 751–767.

Sokolova, Ye. V., Azizov, A. V., Simonov, M. A., Leonyuk, N. I. & Belov, N. V. (1978). *Dokl. Akad. Nauk SSSR*, **243**, 655–658.

Voll, D., Lengauer, C., Beran, A. & Schneider, H. (2001). *Eur. J. Mineral.* **13**, 591–604.

Wada, H., Sakane, K., Kitamura, T., Sunai, M. & Sasaki, N. (1993). *J. Mater. Sci. Lett.* **12**, 1735–1737.

Wang, J., Sha, J., Yang, Q., Wang, Y. W. & Yang, D. R. (2005). *Mater. Res. Bull.* **40**, 1551–1557.

Wells, A. F. (1975). *Structural Inorganic Chemistry*, 4th ed., p. 854. Oxford University Press.

Werding, G. & Schreyer, W. (1984). *Geochim. Cosmochim. Acta*, **48**, 1331–1344.

Werding, G. & Schreyer, W. (1992). *Eur. J. Mineral.* **4**, 193–207.

Werding, G. & Schreyer, W. (1996). *Rev. Mineral. Geochem.* **33**, 117–163.

Yang, T., Ju, J., Li, G. B., Liao, F. H., Zou, X. D., Deng, F., Chen, L., Wang, Y. X. & Lin, J. H. (2007). *Inorg. Chem.* **46**, 4772–4774.